Conformation of spin-labeled melittin at membrane surfaces investigated by pulse saturation recovery and continuous wave power saturation electron paramagnetic resonance

Christian Altenbach,* Wojciech Froncisz,‡§ James S. Hyde,‡ and Wayne L. Hubbell*

*Jules Stein Eye Institute and Department of Chemistry and Biochemistry, University of California Los Angeles, Los Angeles, California 90024-1771; ‡National Biomedical ESR Center, Department of Radiology, Medical College of Wisconsin, Milwaukee, Wisconsin 53226; and §Department of Biophysics, Institute of Molecular Biology, Jagiellonian University, 31-120 Krakow, Poland

ABSTRACT Melittin spin-labeled specifically with a nitroxide at positions 7, 21, 23, or the amino terminus was bound to phospholipid membranes, and the exposure of the spin label to the aqueous phase was investigated by measurement of Heisenberg exchange with chromium oxalate in the solution. The exchange frequency was determined by saturation recovery electron paramagnetic resonance (EPR) using a loop-gap resonator. This method allows use of very low concentrations (<1 mM) of chromium oxalate compared with conventional measurements of EPR line broadening (typically 50 mM), thus avoiding problems associated with high metal ion concentration. Differences in exchange frequency between the various positions were also estimated by continuous wave power saturation methods. In either approach, the spin label at lysine 7 was found to be the most exposed to chromium oxalate whereas that at lysine 23 was found to be the least exposed. This is consistent with a model for the membrane bound peptide in which an amphiphilic helix lies with its axis parallel to the bilayer surface and the hydrophobic moment points toward the bilayer interior.

INTRODUCTION

Melittin is a 26-amino acid peptide found in high concentrations in bee venom (Bernheimer and Rudy, 1986). The protein induces structural changes that lead to enhanced ionic permeability in liposomes (Dufourcq et al., 1984) and intact erythrocytes (DeGrado et al., 1982), and some reports indicate the formation of voltage-dependent channels (Tosteson and Tosteson, 1981; Hanke et al., 1983). The primary structure of melittin is as shown below:

$$\overset{+}{H_3N}\text{—G—I—G—A—V—L—}\overset{+}{K}\text{—V—L—T—T—G—L—P}$$
$$\qquad\quad 1 \qquad\qquad\qquad\qquad 7$$
$$\text{—A—L—I—S—W—L—}\overset{+}{K}\text{—}\overset{+}{R}\text{—}\overset{+}{K}\text{—}\overset{+}{R}\text{—Q—Q—CONH}_2$$
$$\qquad\qquad\qquad\qquad\quad 21 \quad 23$$

In solution at low ionic strength, the peptide has no regular secondary structure. At high ionic strengths, tetramers of melittin form in which each monomer is α-helical (Quay and Condie, 1983). The crystal structure of the tetramer has been determined (Terwilliger and Eisenberg, 1982*a*, *b*). The tetramer is stabilized by hydrophobic interactions between the amphiphilic α-helical subunits.

Melittin binds strongly to phospholipid bilayers, and the structure of the membrane bound state has been a subject of considerable interest. It is generally agreed that the membrane bound peptide is α-helical, but there is no general agreement regarding the organization of the helix within the membrane (Hermetter and Lakowicz, 1986; Vogel and Jaehnig, 1986; Talbot et al., 1987; Altenbach and Hubbell, 1988; Altenbach et al., 1988). Recently, Altenbach and Hubbell (1988) prepared a series of melittins spin-labeled at lysine 7, 21, 23 or at the amino terminus. Each of the derivatives showed hemolytic activity comparable to the native protein, and electron paramagnetic resonance (EPR) investigations showed the molecules to be monomeric at membrane surfaces.

In the present communication these spin-labeled melittins are used to investigate the exposure of specific side chains to the aqueous phase in the membrane-bound protein. This information is then used to evaluate specific models for the orientation and dynamics of the amphipathic helix at the membrane solution interface. The exposure of the nitroxide group of a spin-labeled melittin to the aqueous phase is determined by measurement of the collision frequency of the nitroxide moiety with chromium (III) oxalate (CROX) in the aqueous phase (Berg and Nesbitt, 1979; Yager et al., 1979). CROX is insoluble in the membrane hydrophobic interior and can undergo collisions only with nitroxides directly exposed to the aqueous phase. Collisions of the nitroxide with CROX result in a decrease in the effective spin-lattice relaxation time (T_1) and direct determination of T_1 as a function of CROX concentration provides a convenient measure of nitroxide exposure to the aqueous phase. Conventional approaches to estimate collision frequencies rely on measurement of spectral line widths which depend on T_2, the spin-spin relaxation time. This is a much less sensitive

0006-3495/89/12/1183/09 $2.00

approach since T_2 is considerably shorter than T_1 and is measurably affected only at much higher ($\times$10–100) collision frequencies. Thus T_1 measurements allow the use of much lower CROX concentration (<1 mM). This is important, since high concentrations of CROX affect the ionic strength of the medium and could perturb the organization and interactions of ionic structures at the membrane surface.

This paper reports the first application of direct T_1 measurements by saturation recovery to the investigation of topography in membrane proteins. The results demonstrate the feasibility of such measurements with a sensitivity consistent with the requirements of biological systems.

Changes in nitroxide T_1 relaxation times due to collision with CROX can also be estimated by continuous wave (CW) power saturation methods (Castner, 1959; Poole and Farach, 1971; Poole, 1983; Altenbach et al., 1989). Although this is a more qualitative approach than saturation recovery for nitroxides, it is sensitive and can be carried out on commercial spectrometers. In this study, the results from CW saturation studies are compared with those derived from the more interpretable saturation recovery approach.

THEORY

When a nitroxide and another paramagnetic species such as CROX collide with the proper geometry, Heisenberg exchange occurs (For a review see Molin et al., 1980). Since the spin-lattice relaxation rate ($1/T_1$) of CROX is much faster than that for the nitroxide, this "exchange reagent" is effectively part of the lattice and the exchange is indistinguishable from a nitroxide spin-lattice relaxation event. It is also true that dipolar interactions between spins in solution will induce spin lattice relaxation. A number of experiments indicate that Heisenberg exchange is a dominant mechanism for spin labels and transition metals in solution of viscosity of the order of 1 cP (Hyde and Sarna, 1978). In the present experiments, where the metal ion is in solution and the spin label on a surface, dipolar interactions could possibly contribute to T_1, although Heisenberg exchange is assumed to be dominant.

The effective relaxation rate due to Heisenberg exchange is given by:

$$\frac{1}{T_1} = \frac{1}{T_1^\circ} + f \cdot p \cdot \omega, \tag{1}$$

where T_1° is the spin lattice relaxation time for the nitroxide in the absence of an exchange reagent, p is a measure of the collision efficiency ($p \simeq 1$), f is a statistical correction that depends on the spin states of the colliding species (Subczynski and Hyde, 1981), and ω is the collision frequency in hertz. The collision frequency depends on the diffusion constants of both the nitroxide and exchange reagent, the accessibility of the nitroxide, and the concentration of the exchange reagent. Since ω is directly proportional to the concentration of exchange reagent ($[R]$), $1/T_1$ is a linear function of $[R]$:

$$\frac{1}{T_1} = \frac{1}{T_1^\circ} + \beta \cdot [R], \tag{2}$$

where β is a constant for a particular system at constant temperature and pressure and is a measure of nitroxide accessibility. If a nitroxide is located within a bilayer, collisions of CROX with the membrane surface will only be effective if there are structural fluctuations which periodically expose the nitroxide or permit entry of CROX. If such fluctuations are improbable, a low value of β would result. If a nitroxide is in equilibrium between two different conformations of different accessibility, the experimentally determined value of T_1 in the presence of an exchange reagent will depend on the interconversion rate between the two populations. If the interconversion rate is slow compared to T_1, two populations will be observed. A complete analysis of all possible cases has been made (Yin, 1987).

Pulse saturation recovery EPR directly measures T_1, and is thus an ideal approach for investigating accessibility of nitroxides to collision with exchange reagents. CW power saturation methods can also be used to obtain relative accessibilities under suitable conditions. In this method, the EPR signal amplitude is determined as a function of microwave power up to powers sufficiently high to observe saturation of the spin system. An empirical experimental parameter commonly used to characterize such saturation behavior is $P_{1/2}$, the power at which the signal amplitude is half that it would be if no saturation occurred. For a system that is described by the Bloch equations and exhibits a homogeneous Lorentzian line shape, $P_{1/2}$ is proportional to the inverse product of the effective relaxation times,

$$P_{1/2} = \frac{C}{T_1 \cdot T_2}, \tag{3}$$

where C is a constant for a particular experimental system (Poole, 1983). Combining Eqs. 2 and 3,

$$P_{1/2} \cdot T_2 = P_{1/2}^\circ \cdot T_2^\circ + \beta \cdot C \cdot [R], \tag{4}$$

where $^\circ$ indicates the values in the absence of exchange reagents. Heisenberg exchange between a nitroxide and a fast-relaxing paramagnetic compound like CROX or oxygen leads to equal changes in both $1/T_1$ and $1/T_2$. If $1/T_2$ is much larger than both $1/T_1$ and ω, T_2 is essen-

tially constant and

$$P_{1/2} = P^{\circ}_{1/2} + \beta' \cdot [R] \quad (5)$$

where $\beta' = \beta \cdot C/T_2$.

A plot of $P_{1/2}$ vs. $[R]$ then yields a straight line with slope β' and intercept $P^{\circ}_{1/2}$ similar to Eq. 2. Unlike β, the parameter β' is not a direct measure of accessibility. The parameter β' will be proportional to the accessibility parameter β only if nitroxides with similar T_2 are compared. This is a distinct disadvantage to the $P_{1/2}$ approach in comparison to direct T_1 determination by saturation recovery.

The above expressions apply to spin systems that are described by the Bloch equations and have a homogeneous Lorentzian line shape. Slow motional nitroxide spectra are complex, and it is not obvious that the above simple model should apply. However, one conclusion of the present work is that the simple model adequately describes the saturation behavior of the nitroxides. In particular, relative accessibilities determined for nitroxides of similar lineshape obtained by CW power saturation are in complete agreement with those determined from the saturation recovery measurements which have a solid theoretical foundation.

EXPERIMENTAL

Saturation recovery and CW saturation measurements

Saturation recovery measurements of spin-lattice relaxation times were made on a pulse EPR spectrometer by using equipment (Huisjen and Hyde, 1974 *a*, *b*; Percival and Hyde, 1975) and methods (Hyde, 1979) described previously. Samples were deoxygenated by passing nitrogen around a sample capillary fabricated of TPX, a gas-permeable plastic (Wilmad Glass Co., Inc., Buena, NJ). 20 min were sufficient to equilibrate the sample in the capillary with the surrounding gas. All measurements of saturation recovery were made on the $M_I = 0$ line using a loop-gap resonator (Froncisz and Hyde, 1982; Hubbell et al., 1987). Typically, a pulse width of 1 μs was used for saturation. Pump power was selected to maximize the amplitude of the decay and was typically 50 mW. Observe power was selected to be as high as possible without affecting the time constant of the recovery. Data were fit to a multiple exponential decay using the method of least squares. β was then determined by linear regression analysis of $1/T_1$ vs. [CROX].

CW saturation curves were obtained on a spectrometer system (model E-109, Varian Associates, Inc., Palo Alto, CA) operating at X-band and fitted with a two-loop one-gap resonator and modified as previously described (Hubbell et al., 1987). The field modulation frequency was 100 kHz. Samples were deoxygenated by passing nitrogen around a sample capillary fabricated of TPX. 20 min were sufficient to equilibrate the sample in the capillary with the surrounding gas. For the oxygen exchange experiments, nitrogen gas was replaced with 100% oxygen. Peak-to-peak amplitudes of first-derivative signals (Y') were obtained as a function of incident microwave power in the range of 0.1 to 200 mW. For the loop-gap resonator used, this corresponds to H_1 values between 4.5 and 200 μT. Loop-gap resonators have the advantage that H_1 is homogeneous thus giving uniform saturation over the entire sample. $P_{1/2}$ values were obtained by fitting the amplitude-power data to a function of the form (Poole, 1983)

$$Y' = N \cdot \frac{\Lambda \cdot \sqrt{P}}{(1 + \Lambda^2 \cdot P \cdot \gamma^2 \cdot T_1 \cdot T_2)^{1.5}}, \quad (6)$$

where Λ is an instrumental calibration for the conversion of incident microwave power to microwave magnetic field H_1 ($H_1 = \Lambda \cdot \sqrt{P}$) and γ the gyromagnetic ratio. The $\gamma^2 \cdot T_1 \cdot T_2$ product and the normalization factor N were used as the adjustable parameters. In some instances, it was necessary to use two terms of the form of Eq. 6 with different values of N and $\gamma^2 \cdot T_1 \cdot T_2$. Y' was plotted vs. $\sqrt{P}$ to obtain a so called power saturation curve. $P_{1/2}$ was found as the intersection of the power saturation curve with a straight line of half the initial slope (see Fig. 5). Eq. 6 theoretically describes the power saturation behavior of the first-derivative peak–peak amplitude of a homogeneous Lorentzian line.

Preparation of samples

Melittin (Sigma Chemical Co., St. Louis, MO) was spin labeled at lysine 7, 21, 23, or the NH_2-terminal amino group and purified as described previously (Altenbach and Hubbell, 1988). Egg phosphatidylcholine (PC) was purified from fresh egg yolks according to Singleton (1965).

Unilamellar phospholipid vesicles were prepared by extrusion of egg PC in 10 mM morpholino propane sulfonic acid (MOPS), pH 7, containing 100 mM NaCl through a 1,000-Å filter ("The Extruder," Lipex Biomembranes, Vancouver, B.C., Canada). The concentration of lipid in the vesicle suspension was approximately 50 mg/ml. Melittin was added to the vesicle suspension from a stock solution so that the final ratio of melittin to lipid was 1:50 wt/wt. This corresponds to ~200 lipids per melittin. Conventional EPR spectra of the labeled melittin in solution and bound to the vesicles were as reported earlier (Altenbach and Hubbell, 1988) and confirmed essentially complete binding to the vesicles under all conditions employed here. Measurements of monomeric melittin (1 mg/ml) in the absence of membranes were carried out in 10 mM MOPS, pH 7.

RESULTS AND DISCUSSION

Fig. 1 shows an example of a representative saturation recovery signal from a spin-labeled melittin bound to PC vesicles. The total amount of melittin used for the measurement was ~300 pmol and the total acquisition time was 5 min. In all but one case to be discussed below, the signals were fit well with a single exponential. In general, one expects to observe a sum of exponentials in the recovery signal, one for each relaxation pathway. For the correlation times encountered here, nuclear spin-lattice relaxation is so rapid that the three nitroxide lines are strongly coupled and a single exponential is in fact expected (Yin and Hyde, 1987). This is an important conclusion since the observation of multiple exponentials then implies the existence of multiple spin populations with different effective spin-lattice relaxation times. Fig. 2 shows representative plots of the relaxation rates ($1/T_1$) vs. concentration of CROX in the aqueous solu-

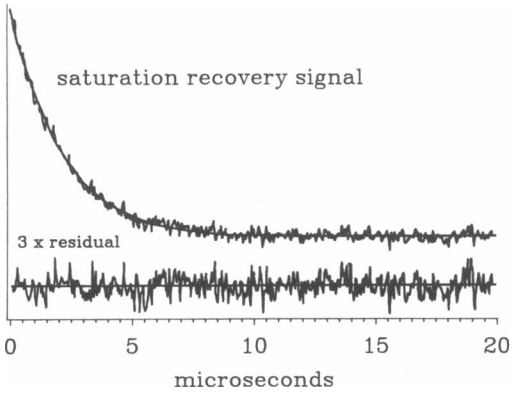

FIGURE 1. Saturation recovery EPR signal. The top part shows the recovery of the EPR signal after a saturating microwave pulse. The vertical axis is inverted. The solid line indicates the fit to a single exponential curve with a time constant off T_1. The difference between experimental data and exponential fit is shown in the lower part.

tion for membrane-bound melittin labeled at position 7 or 23. The rates, and hence collision frequencies, are tolerably linear in concentration. For each of the four melittin derivatives, both free and membrane bound, recovery signals were obtained as a function of CROX concentration between 0 and 1 mM. The data was analyzed as shown in Fig. 2, and the slopes and intercepts of the linear least square fits are given in Table 1. The slopes of the plots, β, are a direct measure for the "specific exchange frequency," i.e., the exchange frequency per millimolar concentration according to Eq. 2. β is a direct measure of label accessibility to the aqueous phase.

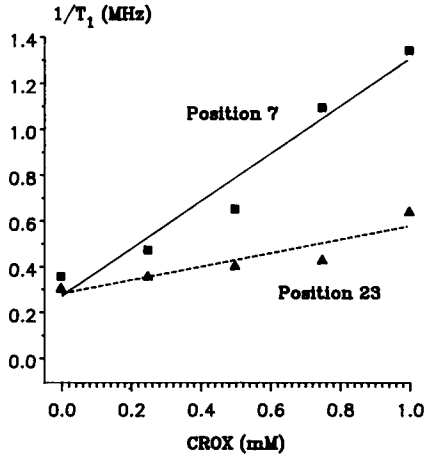

FIGURE 2. Plot of $1/T_1$ vs. concentration of chromium oxalate (*CROX*) for melittin spin labeled at lysine 7 or lysine 23 as measured with saturation recovery EPR spectroscopy. Lysine 7 shows a much steeper dependence and is therefore more exposed to collisions with chromium oxalate.

TABLE 1 CROX accessibility data from saturation recovery EPR measurements of spin labeled melittin bound to membranes and free in solution

	Membrane bound		In solution	
	β	$1/T_1°$	β	$1/T_1°$
	MHz/mM	*MHz*	*MHz/mM*	*MHz*
Mellittin-N-SL				
fast	0.62 ± 0.11	0.34 ± 0.07	5.17 ± 0.61	0.77 ± 0.11
slow	0.13 ± 0.04	0.28 ± 0.03		
Melittin-7-SL	1.04 ± 0.13	0.27 ± 0.08	4.43 ± 0.70	0.71 ± 0.12
Melittin-21-SL	0.76 ± 0.16	0.22 ± 0.10	5.82 ± 0.92	0.69 ± 0.16
Melittin-23-SL	0.30 ± 0.08	0.28 ± 0.05	6.09 ± 0.95	0.64 ± 0.17
C12Q	1.14 ± 0.20	0.26 ± 0.18	7.00 ± 0.52	1.24 ± 0.09

See text and Eq. 2. Membrane-bound melittin labeled at the aminoterminus showed two equal populations with different accessibility. The results for the model compound C12Q is included for comparison. The errors are ±SD and obtained from a statiscal analysis of the linear least square fits.

As can be seen from Table 1, all labeled positions in the free random coil peptide have similar values of β and are thus similarly accessible to CROX. The relatively high errors in the slopes (10–15%) are due to the short relaxation times observed for the free peptide. The slightly higher values for lysine 21 and 23 can be explained by electrostatic considerations (see below). Upon binding to the membrane, all β values decrease by roughly an order of magnitude although significant differences between the individual sites are apparent.

The overall reduction in the specific collision frequency upon membrane binding is expected for at least two reasons. First, the collision frequency between CROX and the nitroxide is linear in the sum of the diffusion constants of the two species according to the Smoluchowski equation, and the diffusion constant of melittin decreases substantially upon binding to the membrane surface. Secondly, the solid angle of approach for a CROX to melittin has been reduced compared to free solution.

In order to aid in interpreting the relative accessibilities of nitroxides on melittin in solution and bound to membranes, the β parameter for an androstane spin-label (*N*-oxyl-4',4'-dimethyloxazolidine derivative of 5α-androstan-3-one-17β-ol, Hubbell and McConnell, 1969) and for the simple amphiphile (I) was investigated.

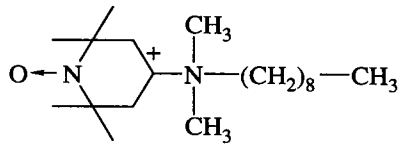

(I)

Spin label (I) binds strongly to membrane surfaces by virtue of the hydrocarbon chain, but the nitroxide function remains in the aqueous phase at the membrane-solution interface (Hubbell et al., 1970; Castle and Hubbell, 1975). The exchange rate of CROX with (I) free in solution is only slightly faster than that for CROX with the various melittin derivatives free in solution. For (I) bound to the membrane, β is reduced to a value similar to that for membrane-bound melittin labeled at position 7. Thus, a large reduction in β upon binding to a surface is characteristic of simple small molecules as well as the peptide and can be understood in terms of reduction of collision rate due to steric constraints imposed by the interface and reduction of diffusion constant. CROX has no effect on the androstane spin-label where the nitroxide group is buried ~12 Å inside the hydrophobic part of the bilayer ($\beta = 0$). This indicates that CROX cannot enter the hydrophobic interior of the membrane.

Of particular interest for the present investigation are the differences between β values for the various label positions in the membrane bound state of melittin. Position 7 has the largest β value and is thus apparently most exposed to collision with CROX. The β value for this derivative is essentially identical with that for the membrane-bound state of (I), which is freely exposed to the aqueous phase. The least exposed is the label at position 23, which has a β value three to four times smaller than that of 7.

The other positions are intermediate. The apparent order of accessibility is $23 < N < 21 < 7$. The saturation recovery signal for the amino-terminal label could be fit with a minimum of two exponentials of approximately equal amplitude. These two components are attributed to two populations of the label. The analysis of the two relaxation rates is shown in Fig. 3. Apparently, the amino-terminal has two conformations in slow exchange on a megahertz time scale, one more buried in the membrane interior. Since this label is rigidly attached to the α-helix backbone by a hydrogen bond (Altenbach and Hubbell, 1988), this would apply to the entire amino-terminal segment of melittin. Alternatively, molecular modeling indicates that the bond connecting the nitroxide ring may exist in two conformations with a rotational barrier high enough to prevent rapid interconversion. In one conformation, the nitroxide group points more toward the membrane and two populations with different accessibility are expected.

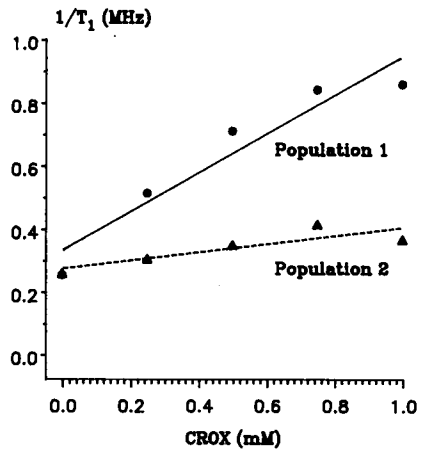

FIGURE 3. Plot of $1/T_1$ vs. concentration of chromium oxalate (*CROX*) for melittin labeled at the amino terminus as measured with saturation recovery EPR spectroscopy. This label shows two different populations with approximately equal amplitude but different accessibility.

In the above discussion, it has been implicitly assumed that the collision frequency is entirely determined by the accessibility of the label. However, CROX is anionic, and the local concentration and exchange frequency should thus be affected by a local electrostatic potential as well as accessibility. To minimize such effects, experiments were conducted at salt concentrations no lower than 0.1 M, and neutral phospholipids were used to form the membranes.[1] If electrostatic effects were observed, they would always be in the direction to enhance the collision frequency since melittin contains only cationic side chains (see primary structure above). The largest electrostatic enhancement would be observed for labels at positions 21 and 23 in the carboxyl-terminal domain which contains three positive charges for the labeled molecule (attachment of the spin label to a lysine removes the charge at that lysine). Such an enhancement explains the higher collision frequencies at these positions in monomeric melittin in solution of low ionic strength. However, a major conclusion of the work is that the collision frequency of CROX with 23 is low relative to free solution or with a spin label at position 7. Thus, if electrostatic effects are present, this conclusion would only be strengthened.

The above results are consistent with an orientation of the melittin helical axis parallel to the membrane surface and with the hydrophobic surface facing the bilayer interior. This orientation, shown in Fig. 4, is similar to that suggested by several authors (Terwilliger et al., 1982; Brown et al., 1982; Stanislawski and Rüterjans, 1987; Altenbach and Hubbell, 1988). The limited accessibility of lysine 23 consistent with its location on the hydrophobic side of the amphipathic α-helix suggests, that this residue is in an α-helical structure. Partial

[1]The actual electrostatic charge on CROX is unknown, but probably near −1. This conclusion is based on vapor pressure measurements of CROX solutions and the dependence of line broadening on ionic strength in solutions of CROX and charged nitroxides (A. P. Todd and W. L. Hubbell, unpublished results).

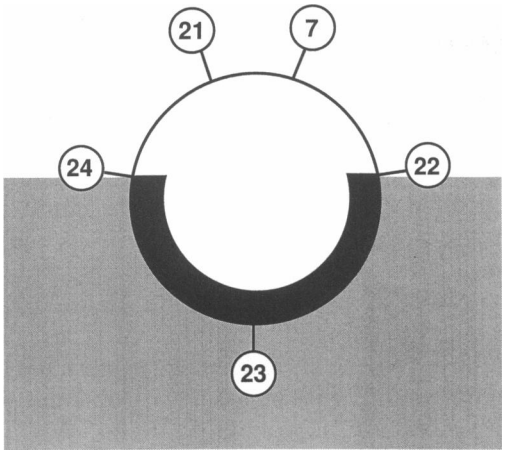

FIGURE 4. Proposed orientation of membrane-bound melittin consistent with the experimental data. This simplified helical projection shows only the charged side chains. The hydrophobic face pointing towards the membrane is indicated by the black area. Lysine 23 points in the direction of the hydrophobic moment and is most buried in the membrane, whereas lysine 7 is most exposed. However, even lysine 23 shows significant exposure and is not truly buried. This can be explained by fluctuations in the orientation and by the length and flexibility of the lysine side chain.

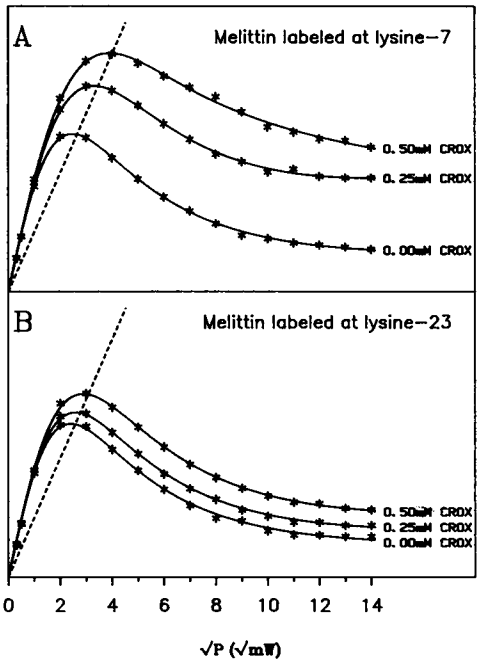

FIGURE 5. Saturation curves as measured with CW saturation EPR spectroscopy. The y-axis is the first derivative EPR signal amplitude and the x-axis is the square root of the incident microwave power. The solid lines show the results of the nonlinear least squares fit according to Eq. 6. (A) Saturation curves of melittin labeled at lysine 7 for various chromium oxalate concentrations as indicated on the right. The dashed line has half the initial slope of the saturation curves and intersects the saturation curve at $\sqrt{P_{1/2}}$. The increase in $P_{1/2}$ with small concentrations of chromium oxalate is evident. At low power there was no difference in EPR signal shape and amplitude at these chromium oxalate concentrations. (B) As in A but with melittin labeled at lysine 23. The effect of chromium oxalate is smaller than in A. Lysine 23 is less exposed to collisions with the hydrophilic chromium oxalate and therefore more buried in the membrane.

unfolding from the carboxyl-terminal end of the helix would presumably lead to an increased exposure of this site.

The saturation recovery approach gives unambiguous information on the collision frequency of CROX with the nitroxide of interest. We have also investigated the interaction of CROX with the nitroxide using the CW power saturation technique described in the Theory section above. Fig. 5 shows representative saturation curves for membrane-bound melittin labeled at positions 7 and 23 for various concentrations of CROX. It is interesting to note that this saturation data for the $M_I = 0$ line of the complex nitroxide lineshape is extremely well fit by Eq. 6, which is derived for saturation of a simple homogeneous Lorentzian line. In some cases, two terms of the form expressed by Eq. 6 were required for the best fit, but the second term was always small. The intersection of the dotted line with the saturation curves in Fig. 5 gives the value of $P_{1/2}$. It is evident that the effect of CROX on the $P_{1/2}$ value is larger for a nitroxide at position 7 than for one at position 23. Values of $P_{1/2}$ at three different concentrations of CROX were obtained for all derivatives in the membrane-bound state. Plots of $P_{1/2}$ vs. CROX were all linear for this limited data set, as predicted by Eq. 5 for the simple model presented in the Theory section. Values for the intercepts ($P^{\circ}_{1/2}$) and slopes (β) are given in Table 2.

Saturation recovery measurements suggested that the amino-terminal label in the presence of CROX exhibits two populations with different T_1's that differ at most by a factor of 2 (see Fig. 3). With the CW saturation approach, it is not possible to distinguish multiple populations with relaxation times so similar, and only a single value of β' is listed in Table 2.

It is instructive to compare values of β determined from saturation recovery measurements with values of β' determined from CW power saturation. Fig. 6 shows clearly that the relative values of the two parameters are in excellent agreement for the derivatives at positions 7, 21, and 23. The β' parameter for the amino terminal is larger relative to the others than is the β parameter. The spectral lineshape for the 7, 21, and 23 derivatives bound to the membrane are very similar, whereas that for the amino-terminal derivative is considerably broader (Altenbach and Hubbell, 1988). On the basis of the above information, it appears that the β' parameter from CW power saturation can provide correct relative accessibilities of

TABLE 2 **CROX accessibility data from CW power saturation EPR measurements of spin labeled melittin bound to membranes**

	Membrane bound		In solution	
	β'	$P_{1/2}°$	β'	$P_{1/2}°$
	mW/mM	*mW*	*mW/mM*	*mW*
Mellittin-N-SL	28.5 ± 2.3	9.4 ± 0.7		
Melittin-7-SL	18.2 ± 1.0	7.2 ± 0.3		
Melittin-21-SL	13.4 ± 1.7	6.8 ± 0.5	25.7	3.6
Melittin-23-SL	5.7 ± 0.9	6.5 ± 0.3		

See text and Eq. 5.

the nitroxide group for radicals of similar lineshape. Interestingly, this is just the result that would be predicted on the basis of the simple model represented by Eq. 5. Within the framework of this model, similar spectral lineshapes have similar values of T_2 and β' is therefore proportional to β. On the other hand, a broader line shape like that for the amino terminus would have a shorter T_2 and hence leads to a relative overestimation of the accessibility from β'. The case is reversed for melittin free in solution. Here the high mobility indicates a long T_2 that leads to an underestimation of the accessibility. This is what is observed. The quotient β'/β is very similar for membrane-bound melittin labeled at positions 7, 21, and 23 (β'/β = 17.5, 17.6, and 19, respectively) but it is higher for the amino terminus (β'/β = 49–220) and lower for melittin labeled at position 21 free in solution (β'/β = 4.4).

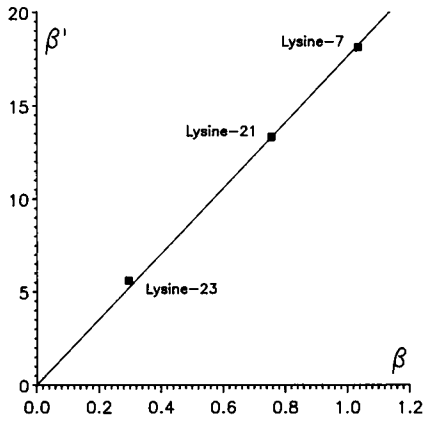

FIGURE 6. Comparison between the accessibility parameters obtained with the two methods of this study. The horizontal axis shows the β parameter in megahertz per millimolar obtained by pulse saturation recovery EPR and the vertical axis shows the β' parameter in milliwatts per millimolar obtained from CW power saturation EPR. Only the spin-labeled lysines have similar spectral lineshape and can be compared directly (see text).

The above discussion has emphasized the inaccessibility of the nitroxide at 23 relative to the others for membrane-bound melittin. However, it should be noted that the nitroxides on all of the derivatives are quite exposed to water. Studies with spin-labeled bacteriorhodopsin (Altenbach et al., 1989) indicate that a spin label attached to a transmembrane segment is much less accessible to CROX. In such a case, CROX concentration as high as 50 mM has no significant effect on $P_{1/2}$. This eliminates any structural models for melittin bound to membranes that involve removal of the side chains from direct access to the aqueous phase.

Another useful probe of topography for membrane proteins is molecular oxygen (Subczynski and Hyde, 1981; Vachon et al., 1987; Altenbach et al., 1989). Like CROX, it is fast relaxing and causes efficient spin lattice relaxation upon collision with a nitroxide. Unlike CROX, it is soluble in both the aqueous and membrane phases, preferring the membrane phase by about 10 to 1 (Wilhelm and Battino, 1973; Wilhelm et al., 1977; Popp and Hyde, 1981; Subczynski and Hyde, 1981, 1983, 1984). Thus it can serve as a probe to identify nitroxide groups exposed to the membrane interior. Table 3 gives values for the change in $P_{1/2}$ caused by switching from a nitrogen to an oxygen atmosphere in equilibrium with the sample. Considering the result obtained with CROX, only the 7, 21, and 23 derivatives with similar lineshape will first be compared with each other. Lysine 7–labeled melittin has the smallest change in $P_{1/2}$, indicating that it experiences the lowest collision frequency with dissolved oxygen. This is clearly not due to steric constraints, since lysine 7 is quite mobile and exposed to collision with the more bulky reagent CROX. Lysine 23–labeled melittin has the greatest change in $P_{1/2}$ on exposure to oxygen, suggesting that it experiences the highest collision frequency. These results are just the inverse of those with CROX and are consistent with the higher solubility of oxygen in the membrane and the locations of lysine 7 and 23 suggested by the CROX studies. Lysine 21 has an intermediate accessibility. Again, the amino-terminal label shows a

TABLE 3 **Accessibility of membrane bound spin labeled melittin to molecular dissolved oxygen as measured with CW power saturation EPR measurements**

	Membrane bound $\Delta P_{1/2}$	In solution $\Delta P_{1/2}$
	mW	*mW*
Mellittin-N-SL	99.5	
Melittin-7-SL	57.9	
Melittin-21-SL	87.9	18.4
Melittin-23-SL	94.0	

See text.

higher apparent exposure consistent with its more immobilized lineshape.

Taken together, these results strongly support the orientation of the melittin helix shown in Fig. 4.

The authors thank Dr. M. Pasienkiewicz-Gierula for much assistance in the computer analysis of the saturation recovery data.

This work was supported by National Institutes of Health grant EY05216 and the Jules Stein Professor endowment to Dr. Hubbell and National Institutes of Health grants RR01008 and GM22923 to Dr. Hyde.

Received for publication 23 March 1989 and in final form 26 June 1989.

REFERENCES

Altenbach, C., S. L. Flitsch, H. G. Khorana, and W. L. Hubbell. 1989. Structural studies on transmembrane proteins. 2. Spin labeling of bacteriorhodopsin mutants at unique cysteins. *Biochemistry.* 28:7806–7812.

Altenbach, C., W. Froncisz, W. L. Hubbell, and J. S. Hyde. 1988. The orientation of membrane bound, spin labeled melittin as determined by EPR saturation recovery measurements. *Biophys. J.* 53:94*a*. (Abstr.)

Altenbach, C., and W. L. Hubbell. 1988. The aggregation state of spin-labeled melittin in solution and bound to phospholipid membranes: evidence that membrane bound melittin is monomeric. *Proteins Struct. Funct. Genet.* 3:230–242.

Berg, S. P., and D. M. Nesbitt. 1979. Chromium oxalate: a new spin label broadening agent for use with thylakoids. *Biochim. Biophys. Acta.* 548:608–615.

Bernheimer, A. W., and B. Rudy. 1986. Interactions between membranes and cytolytic peptides. *Biochim. Biophys. Acta.* 864:123–141.

Brown, L. R., W. Braun, A. Kumar, and K. Wüthrich. 1982. High resolution nuclear magnetic resonance studies of the conformation and orientation of melittin bound to a lipid-water interface. *Biophys. J.* 37:319–328.

Castle, J. D., and W. L. Hubbell. 1975. Estimation of membrane surface potential and charge density from the phase equilibrium of a paramagnetic amphiphile. *Biochemistry.* 15:4818–4831.

Castner, T. G. 1959. Saturation of the paramagnetic resonance of a V center. *Phys. Rev.* 115:1506–1515.

DeGrado, W. F., G. F. Musso, M. Lieber, E. T. Kaiser, and F. J. Kézdy. 1982. Kinetics and mechanism of hemolysis induced by melittin and by a synthetic melittin analogue. *Biophys. J.* 37:329–338.

Dufourcq, J., J. L. Dasseux, and J. F. Faucon. 1984. An illustrative model for lipid-protein interactions in membranes: a review of melittin-phospholipid systems. In *Bacterial Protein Toxins.* Academic Press, Ltd., London. 127–138.

Froncisz, W., and J. S. Hyde. 1982. The loop-gap resonator: A new microwave lumped circuit ESR sample structure. *J. Magn. Resonance.* 47:515–521.

Hanke, W., C. Methfessel, H. U. Wilmsen, E. Katz, G. Jung, and G. Boheim. 1983. Melittin and a chemically modified trichotoxin form alamethicin-type multi-state pores. *Biochim. Biophys. Acta.*727:108–114.

Hermetter, A., and J. R. Lakovicz. 1986. The aggregation state of melittin in lipid bilayers. An energy transfer study. *J. Biol. Chem.* 261:8243–8248.

Hubbell, W. L., W. Froncisz, and J. S. Hyde. 1987. Continuous and stopped flow EPR spectrometer based on a loop gap resonator. *Rev. Sci. Instrum.* 58:1879–1886.

Hubbell, W. L., and H. M. McConnell. 1969. Motion of steroid spin labels in membranes. *Proc. Natl. Acad. Sci. USA.* 63:16–22.

Hubbell, W. L., J. C. Metcalfe, S. M. Metcalfe, and H. M. McConnell. 1970. The interaction of small molecules with spin labelled erythrocyte membranes. *Biochim. Biophys. Acta.* 219:415–427.

Huisjen, M., and J. S. Hyde. 1974*a*. A pulsed EPR spectrometer. *Rev. Sci. Instrum.* 45:669.

Huisjen, M., and J. S. Hyde. 1974*b*. Saturation recovery measurements of electron spin-lattice relaxation times of free radicals in solutions. *J. Chem. Phys.* 60:1682.

Hyde, J. S. 1979. *In Time Domain Electron Spin Resonance.* L. Kevin and R. M. Schwartz, editors. John Wiley & Sons, New York. 1–30.

Hyde, J. S., W. Froncisz, and C. Mottley. 1984. Pulsed measurement of nitrogen T_1 in spin labels. *Chem. Phys. Lett.* 110:621–625.

Hyde, J. S., and T. Sarna. 1978. Magnetic interactions between nitroxide free radicals and lanthanides or Cu^{2+} in liquids. *J. Chem. Phys.* 68:4439–4447.

Molin, Yu. N., K. M. Salikhov, and K. I. Zamaraev. 1980. Spin exchange. Springer-Verlag, Berlin.

Percival, P. W., and J. S. Hyde. 1975. Pulsed EPR spectrometer, II. *Rev. Sci. Instrum.* 46:1522.

Poole, C. P. 1983. *Electron Spin Resonance.* John Wiley & Sons, New York.

Poole, C. P., and H. A. Farach. 1971. *Relaxation in Magnetic Resonance.* Academic Press, Inc., New York.

Popp, C. A., and J. S. Hyde. 1981. Effects of oxygen on EPR spectra of nitroxide spin-label probes of model membranes. *J. Magn. Resonance.* 43:249–258.

Quay, S. C., and C. C. Condie. 1983. Conformational studies of aqueous melittin: thermodynamic parameters of the monomer tetramer self-association reaction. *Biochemistry.* 22:695–700.

Singleton, W. S., M. S. Gray, M. L. Brown, and J. L. White. 1965. Chromatographic homogenous lecithin from egg phospholipids. *J. Am. Oil Chem. Soc.* 42:53–57.

Stanislawski, B., and H. Rüterjans. 1987. ^{13}C-NMR investigation of the insertion of the bee venom melittin into lecithin vesicles. *Eur. Biophys. J.* 15:1–12.

Subczynski, W. K., and J. S. Hyde. 1981. The diffusion-concentration product of oxygen in lipid bilayers using the spin-label T_1 method. *Biochim. Biophys. Acta.* 643:283–291.

Subczynski, W. K., and J. S. Hyde. 1983. Concentration of oxygen in lipid bilayers using a spin-label method. *Biophys. J.* 41:283–286.

Subczynski, W. K., and J. S. Hyde. 1984. Diffusion of oxygen in water and hydrocarbons using an electron spin resonance spin-label technique. *Biophys. J.* 45:743–748.

Talbot, J. C., J. F. Faucon, and J. Dufourcq. 1987. Different states of self-association of melittin in phospholipid bilayers: a resonance energy transfer approach. *Eur. Biophys. J.* 15:147–157.

Terwilliger, T. C., and D. Eisenberg. 1982*a*. Structure of melittin. 1. Structure determination and partial refinement. *J. Biol. Chem.* 257:6010–6015.

Terwilliger, T. C., and D. Eisenberg. 1982*b*. Structure of melittin. 2. Interpretation of the structure. *J. Biol. Chem.* 257:6016–6022.

Terwilliger, T. C., L. Weissman, and D. Eisenberg. 1982. The structure of melittin in the form I crystals and its implication for melittin's lytic and surface activities. *Biophys. J.* 37:353–361.

Tosteson, M. T., and D. C. Tosteson. 1981. The sting: melittin forms channels in lipid bilayers. *Biophys. J.* 36:109–116.

Vachon, A., C. Lecomte, F. Berleur, V. Roman, M. Fatome, and P. Braquet. 1987. Oxygen diffusion-concentration in phospholipidic model membranes. *J. Chem. Soc. Faraday Trans.* 1:83:177–190.

Vogel, H., and F. Jaehnig. 1986. The structure of melittin in membranes. *Biophys. J.* 50:573–582.

Wilhelm, E., and R. Battino. 1973. Thermodynamic functions of the solubilities of gases in liquids at 25°C. *Chem. Rev.* 73:1–9.

Wilhelm, E., R. Battino, and R. J. Wilcock. 1977. Low pressure solubility of gases in liquid water. *Chem. Rev.* 77:219–262.

Yager, T. D., G. R. Eaton, and S. S. Eaton. 1979. Metal-nitroxyl interactions. 12. Nitroxyl spin probes in the presence of tris(oxalato)chromate(III). *Inorg. Chem.* 18:725–727.

Yin, J. J. 1987. Mathematical models of spin dynamics in spin labeled membranous systems with experimental verifications using CW ELDOR and pulse saturation recovery electron spin resonance. Doctoral dissertation, Medical College of Wisconsin.

Yin, J. J., and J. S. Hyde. 1987. Spin-label saturation recovery electron spin resonance measurement of oxygen transport in membranes. *Z. Phys. Chem.* 153:57–65; 541–549.